

The HST Medium Deep Survey Cluster Sample: Methodology and Data

E. J. Ostrander, R. C. Nichol, K. U. Ratnatunga & R. E. Griffiths

Department of Physics, Carnegie Mellon University, 5000 Forbes Ave., Pittsburgh, PA-15213, USA

ABSTRACT

We present a new, objectively selected, sample of galaxy overdensities detected in the Hubble Space Telescope Medium Deep Survey. These clusters/groups were found using an automated procedure which involved searching for statistically significant galaxy overdensities. The contrast of the clusters against the field galaxy population is increased when morphological data is used to search around bulge-dominated galaxies. In total, we present 92 overdensities above a probability threshold of 99.5%. We show, via extensive Monte Carlo simulations, that *at least* 60% of these overdensities are likely to be real clusters and groups and not random line-of-sight superpositions of galaxies. For each overdensity in the MDS cluster sample, we provide a richness and the average of the bulge-to-total ratio of galaxies within each system. This MDS cluster sample potentially contains some of the most distant clusters/groups ever detected, with about 25% of the overdensities having estimated redshifts $z \gtrsim 0.9$. We have made this sample publicly available to facilitate spectroscopic confirmation of these clusters and help more detailed studies of cluster and galaxy evolution.

We also report the serendipitous discovery of a new cluster close on the sky to the rich optical cluster CL0016+16 at $z = 0.546$. This new overdensity, HST 001831+16208, may be coincident with both an X-ray source and a radio source. HST 001831+16208 is the third cluster/group discovered near to CL0016+16 and appears to strengthen the claims of Connolly et al. (1996) of superclustering at high redshift.

Subject headings: catalogs – cosmology: observations – galaxies: clusters: general – galaxies: clusters: individual (CL0016+16, RXJ0018.3+1618, RXJ0018.8+1602) – galaxies: evolution

1. Introduction

Clusters of galaxies¹ are the largest known gravitationally bound objects in the universe. They are key tracers of the large-scale structure in the universe (e.g. Postman, Huchra & Geller 1992) and provide an economical way of surveying large volumes of space. Furthermore, they represent the highest peaks in the underlying mass density field and are therefore sensitive indicators of the mean density of the universe *i.e.* Ω (see Richstone, Loeb & Turner 1992). Clusters of galaxies have become one of the favored tools of theoretical cosmologists as relatively simple analytical methods can be developed to understand the distribution, evolution and formation of clusters (e.g. Press & Schechter 1974). In addition to delineating

¹Throughout this paper, we will use the term “cluster” loosely to represent any statistical overdensity we have detected. This includes a range in richness from groups of galaxies to rich Abell-like clusters.

the large-scale structure, clusters provide a useful laboratory within which to study galaxy evolution as a function of environment.

Classically, clusters/groups of galaxies have been found via visual searches of optical galaxy catalogues for statistical excesses of galaxies above the background population. These galaxy overdensities are then characterized by richness and compactness criteria (a certain surface density of galaxies is usually required). In addition, a measure of the cluster’s absolute brightness is obtained. The first major catalogues of clusters and groups of galaxies were produced by Abell (1958) & Zwicky et al. (1968) from visual scans of optical photographic plates. The Abell catalogue (Abell, Corwin & Olowin 1989) is still widely used in present day astronomical research; it contains more than 4000 nearby clusters, some as far out as $z \simeq 0.4$, and has been shown to be complete to $z \simeq 0.15$ (Huchra et al. 1990). The most widely used catalogue of groups of galaxies is the Hickson catalogue of compact groups (median redshift of $z = 0.03$). The reader is referred to an excellent recent review of the Hickson catalogue – and science extracted from it – by Hickson (1997). Gunn, Hoessel & Oke (1986) were the first to publish a catalogue of distant optical clusters of galaxies, followed by Couch et al. (1991). These catalogues were also constructed from visual scans of deep 4m photographic plates and combined contain 530 candidate clusters/groups out to $z \sim 1$.

All these aforementioned optical cluster catalogues have two severe limitations. First, they are visually-based catalogues and therefore, do not have well-determined selection functions. This hinders a robust measurement of the volume sampled by these surveys. This is a vital quantity which is needed for an unambiguous comparison of the observations with theoretical predictions. Second, a caveat which also applies to the present work, these optical clusters are detected as overdensities in the projected distribution of galaxies *i.e.* in two dimensions. This can result in “phantom” clusters which appear to be clusters on the sky, but are, in reality, superpositions of galaxies along the line-of-sight. Numerical simulations of the contamination by projection effects suggest that up to 50% of all Abell clusters could be spurious (Lucey 1983; Frenk et al. 1990; van Haarlem, Frenk & White 1997)

In recent years, the situation regarding optical catalogues of clusters has changed. The Palomar Distant Cluster Survey (PDCS, Postman et al. 1996) is the first fully automated survey for optical clusters of galaxies and takes advantage of large CCD cameras on 4-metre class telescopes. This makes it possible to survey large areas of the sky to faint magnitude limits. The PDCS covers a total area of 5deg^2 in two bands – V_4 and I_4 – to a completeness magnitude of $I \simeq 22$. Postman et al. used a matched-filter cluster-finding algorithm that detected 107 clusters in total; 79 of which formed a complete sample of clusters in the estimated redshift range of $0.2 < z < 0.6$. Via extensive Monte Carlo simulations, the PDCS has a well-known selection function and therefore, the volume sampled by the survey has been determined. These simulations were also used to determine the completeness of the survey and the likely contamination rate by “phantom clusters” (estimated to be $< 30\%$). In addition to the PDCS, there are several other examples of the use of objective criteria to find and classify optical clusters (see Lumsden et al. 1992; Lidman & Peterson 1996; Kawasaki et al. 1997; Kepner et al. 1998; Kodama, Bell & Bower 1998).

In this paper, we present a new catalogue of distant optical clusters selected objectively from the Hubble Space Telescope (HST) Medium Deep Survey (MDS). The motivation for this new survey is to increase the total number of potentially high redshift clusters. This survey will be known as the MDS Cluster Sample. In Section 2, we briefly summarize the overall MDS methodology and catalog. In Section 3, we discuss the cluster-finding algorithm while in Section 4 we outline the sample of 92 overdensities in the MDS cluster sample. In Section 5, we present the simulations we have performed to assess the robustness of the clusters selected, while in Section 6 we discuss the selection function of the MDS cluster sample. Section 7 we give our discussions and conclusions.

Table 1: Number of HST WFP2 fields used in the MDS cluster sample. Also presented is the effective area (arcmins²) – accounting for field overlaps and edge effects (see text) – as a function of HST passband. The number of galaxies, regardless of their morphology, in each passband is given along with the number of disk-dominated and bulge-dominated galaxies (see text for definitions). The total number of galaxies far exceeds the number of bulge and disk-dominated galaxies because it includes lower signal-to-noise galaxies that were not classified.

Filter	No.	Unique	Total	Morphology	
	Fields	Area	Galaxies	Bulge	Disk
F450W (b)	29	119.6	10070	619	3595
F606W (v)	251	1062.0	69313	5917	27670
F814W (i)	319	1285.1	89790	7118	36649

2. The HST Medium Deep Survey

The MDS is a long-term project dedicated to extracting as much scientific information as possible out of the large amount of parallel data taken by the HST Wide Field and Planetary Camera (WFPC2). For a complete summary of the methodology used in the MDS, the reader is referred to Griffiths et al. (1994) but for completeness, we review the salient points here.

To date, the MDS contains over 800 WFPC2 fields scattered over the whole sky, of which over 500 of the better quality fields have been fully analyzed. The analysis involves a semi-automated data reduction pipeline that is designed to take the raw HST WFPC2 data and produce calibrated catalogues of model-fitted galaxies. The first step involves dark and bias subtraction followed by flat-fielding and hot pixel removal. The images are then added to help remove cosmic-ray events. The reader is referred to Ratnatunga et al. (1994) for a full review of all these procedures.

The second step is object detection which involves a local peak-finding algorithm that locates contiguous pixels one-sigma above a local sky determination. These detected objects are then visually inspected. The third and final step in the MDS analysis is a maximum likelihood model fit for the morphology of the objects in each field. This involves a 2-dimensional Disk+Bulge decomposition of these faint undersampled images and has been shown to provide an unbiased estimate of the real morphology of the sources down to F814W = 22.7, F606W = 23.3 and F450W = 23.1 in a one hour exposure. In this way, the MDS provides reliable morphologies for each detected object *e.g.* stellar, faint galaxy, bulge-like galaxy, disk-like galaxy or a bulge+disk galaxy. The reader is referred to Ratnatunga, Griffiths & Ostrander (1998) for a detailed explanation of this fitting procedure (or see <http://astro.phys.cmu.edu/mds/mle/>).

For the work discussed in this paper, we do not use all available fields in the MDS. A summary of the fields we have used and the composition of their galaxy morphologies is given in Table 1. These MDS fields are scattered over the whole sky but we have excluded all fields at low galactic latitude, $|b| \leq 16^\circ$, to help minimize false detections due to the increased surface density of stars. We have also excluded some high galactic latitude fields dominated by stars (*i.e.* LMC), nearby galaxies (to avoid globular clusters) and MDS fields where the primary target was a known cluster.

Throughout this paper, we use the term “bulge dominated” to describe a galaxy that has a $\geq 50\%$ bulge model component in the MDS 2D morphological model fit as discussed above and in detail in

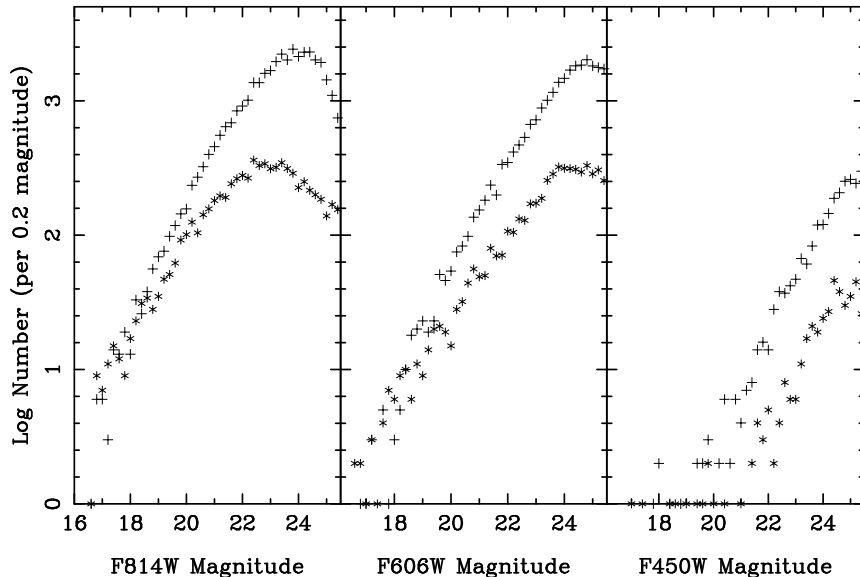


Fig. 1.— The number of galaxies used in this paper as a function of passband, magnitude and morphology. This figure is not meant to be used as the number–magnitude relationship for the whole MDS survey as that has been published elsewhere. The + symbols represent galaxies classified as disk dominated and * represent galaxies classified as bulge dominated. See text for the definition of these two morphological classifications.

Ratnatunga et al. (1994, 1998). In other words, the dominant component of the galaxy profile is a bulge as seen in ellipticals and S0 galaxies. Likewise, we use the term “disk dominated” to describe a galaxy that has $> 50\%$ disk component in the 2D MDS morphological model fit.

In Fig. 1, we present the number of galaxies used in this paper as a function of magnitude, passband and galaxy morphology. This is not meant to be used as a number–magnitude relationship for the whole MDS galaxy survey since this has been published elsewhere (Roche et al. 1998). In Table 2, we present the differential areal coverage, as a function of the completeness limit of each field, for the MDS cluster sample. The field completeness limit is calculated based on the exposure time, number of exposures and the local sky background (see Ratnatunga et al. 1998). The total amount of area covered by the MDS cluster survey, after the removal of overlaps between neighbouring fields, is given in Table 1. These data are vital to the usefulness of the MDS cluster sample as they will be needed for any estimate of the volume sampled by our cluster survey.

Table 2 was computed by summing the number of fields as a function of their limiting magnitude and accounting for overlap between adjacent fields. The degree of overlap was small; for the F814W data only 2% of the area overlapped with an adjacent MDS field. We used the effective total area as defined in Section 6 for the available search area per WFPC2 field (4.27 arcmins²).

3. Construction of the Cluster Sample

Table 2: The differential area of the MDS cluster sample as a function of limiting magnitude (in arcmin²). We have accounted for edge effects (see text)

b-band		v-band		i-band	
mag	area	mag	area	mag	area
24.625	8.54	23.625	12.81	22.625	12.81
24.875	12.81	23.875	15.54	22.875	11.25
25.125	51.24	24.125	95.97	23.125	66.52
25.375	29.89	24.375	160.17	23.375	106.71
25.625	12.81	24.625	193.98	23.625	147.74
26.625	4.27	24.875	106.68	23.875	178.65
		25.125	264.30	24.125	212.72
		25.375	76.86	24.375	330.82
		25.625	55.51	24.625	124.32
		25.875	8.54	24.875	68.32
		27.125	4.27	25.125	4.27
				26.125	4.27

3.1. Overview

The requirements of a cluster-finding algorithm are clear; it must maximize the number of true clusters detected, in a noisy correlated background, while minimizing the number of false detections. Moreover, it should have as simple a definition as possible, allowing the selection function of the cluster survey to be well understood. Ideally, the algorithm would make as few assumptions as possible about the clusters it is trying to detect to minimize possible biases.

The PDCS used a matched-filter technique which involves filtering the data with a physical model of a cluster. This helps to increase the contrast of any cluster as a function of redshift and radius. However, it does impose a particular cluster model on the data. Other techniques have included simply peak-finding within galaxy catalogues (Lumsden et al. 1992), a maximum likelihood method similar to the PDCS algorithm (Kawasaki et al. 1997) and a wavelet-based method (Slezak, Bijaoui & Mars 1990).

The MDS is a unique database of galaxies upon which to build a new search for distant clusters of galaxies. This is primarily because it is the largest collection of galaxy morphologies in existence and we can utilize this morphological information to develop a simple and effective cluster-finding algorithm taking advantage of the density-morphology relationship (Dressler 1980). It has been shown that clusters and groups are dominated by elliptical galaxies whereas the field galaxy population is predominantly made up of spirals. It is therefore possible to greatly enhance the contrast of distant clusters of galaxies against the field population with morphological data.

In addition to the morphological information, the MDS includes some of the deepest photometric data ever obtained, meaning that the MDS cluster sample has, on average, a fainter limiting magnitude than any previous search for distant clusters (see Fig. 1), while still covering a reasonable area of the sky (0.4deg² in F814W, see Table 2). We have included in the search the Hubble Deep Field (HDF; Williams et al. 1996) and the Groth-Westphal strip, since these fields were not selected for any particular target and therefore, should be representative of the galaxy population. Moreover, it allows us to statistically quantify

the existence of any galaxy overdensities in these very deep images.

We note that any cluster/group search based on the morphologies of the galaxies is potentially biased due to evolutionary effects. This may limit the usefulness of the catalogue; for example, detailed studies of the morphological constitution of these MDS distant clusters could be undermined (see Section 6). We believe however, that our algorithm may be robust against such concerns for two reasons. First, we only require one bulge dominated galaxy per cluster *i.e.* one elliptical or S0. Second, bright cluster ellipticals are thought to have formed at very high redshift ($z > 1$) and have evolved passively since then (see Dickinson 1997). Finally, the number of irregular galaxies increases at high redshift which potentially biases our result as we do not search around such galaxies. However, the total number of irregulars detected in the Hubble Deep Field is only $\sim 25\%$ and therefore, we do not envisage this to be a large effect for our shorter exposure MDS fields.

3.2. The Mechanics of the Algorithm

Here we discuss the details of the cluster-finding algorithm. The original plan for our cluster-finding algorithm was to base our search for overdensities on the photometric redshifts of galaxies, allowing us to scale a fixed metric aperture, and a fixed absolute magnitude width, with this redshift. However, our initial investigations of such an algorithm showed that the errors on the photometric redshifts, because of our limited color data, were too high. Moreover, in the redshift range we are probing with this MDS data, $z \simeq 0.5$ to $z \simeq 1$, the angular diameter-redshift relationship is almost flat and therefore, there is little need to scale a metric aperture with redshift.

Our algorithm was based on the search for statistically significant galaxy overdensities in an array of different apertures centered on each bulge dominated galaxy in the MDS. We vary both the radius and the magnitude range of these search apertures (see below) to increase our probability of finding clusters over a large range in redshift. This approach also means that our selection is less biased towards finding clusters with a particular radial profile and/or galaxy luminosity function.

The angular size of the apertures were varied from 10 to 35 arcseconds in radius, in steps of 5 arcseconds, which corresponds to a range of $80 h^{-1}$ kpc to $285 h^{-1}$ kpc in metric diameters for a median redshift of $\simeq 0.75$ (we use $q_0 = 0.5$ and $H_0 = 100 \text{ km s}^{-1} \text{ Mpc}^{-1}$, or $h = 1$ throughout). The magnitude range of the apertures is fixed at 2 magnitudes ($0.5 \leq m_c < 1.5$) but the central magnitude (m_c) is varied, in steps of 0.25 magnitude, from 16.5 magnitudes to 1.5 magnitudes brighter than the completeness limit of each individual field. The bright magnitude limit was chosen based on Fig. 1 which shows there are very few galaxies brighter than this, in all 3 HST passbands, within the MDS database. Therefore, the number of apertures used per ‘seed’ galaxy (the galaxy at the center of the aperture) varies depending on the field, but typically ~ 60 different radius/magnitude apertures are applied. We excluded from the analysis apertures that had less than 75% of their area within the WFPC2 image.

The algorithm used for the MDS cluster sample was broken into two stages. The first stage involved processing all galaxies regardless of their morphology and passband as given in Table 1. For each galaxy, we counted the number of galaxy neighbors in the array of apertures discussed above which resulted in a set of distribution functions that show the frequency of neighboring galaxies as both a function of search radius and magnitude. These functions form the basis for our overdensity search and act as our null hypothesis. They are our determination of the background galaxy population against which we can test the statistical significance of any observed overdensity. Simply put, these distributions represent our measurement of the

galaxy angular correlation function. The second stage of the construction of the MDS cluster sample is very similar to the first stage, however, in this stage we only placed apertures on bulge dominated galaxies and once again counted the number of neighboring galaxies.

We are now faced with a problem that is common to all objective searches for clusters. We need to determine the threshold above which a galaxy overdensity enters our sample. Such a threshold can either be determined empirically by maximizing the number, or type, of cluster one wants to find, or one can simply set an arbitrary threshold. Irrespective of the actual threshold, it is very important to document the decision to provide future users of the catalogue a clear view of what was included and discarded. This will greatly aid comparison with theoretical models.

For the MDS cluster sample, we empirically selected our thresholds – which are richness cutoffs – from the distributions constructed in the first stage discussed above. For each combination of aperture size and magnitude range, we computed the galaxy richness that corresponds to the 99.5 percentile in each distribution *i.e.* the galaxy richness of an overdensity above which it is in the top 0.5% of all galaxy overdensities observed in the MDS. An example of these galaxy richness cutoffs, as a function of radius and magnitude, is given in Table 3. In summary, we have presented all groups/clusters that are in the tail of the distribution.

This percentile cutoff (99.5%) was determined from a visual inspection of the MDS cluster detections. This method does not undermine the objectivity of the cluster selection since, above this chosen percentile threshold, all detected overdensities, regardless of their subjective visual appearance, are included. The threshold corresponds to an arbitrary richness (or mass) cutoff that can be solidified later via multi-object spectroscopy.

At the end of the second stage, nearly a thousand cluster candidates were detected above the richness cutoffs discussed above and shown in Table 3. They were separated into 3 catalogues, one for each of the HST passbands. This large number of candidate clusters is simply a reflection of the same real clusters being found many times over as each bulge dominated galaxy in a cluster can provide a potential detection. Overlaps were removed by sorting the catalogues, as a function of passband, and finding any candidates that had the same central right ascension and declination within a radius of 30 arcseconds. For these common candidates, the one with the highest detection percentile was chosen as the main cluster detection. If the candidates had the same detection percentile, then the one with the highest galaxy richness was taken. Once the cluster catalogues for the individual passbands were sorted, they were combined using the same sorting algorithm *i.e.* if two candidates, in different passbands, had the same central right ascension and declination within a radius of 30 arcseconds, the candidate with the highest detection percentile was chosen. If the candidates had the same detection percentile, then the one with the highest galaxy richness was taken.

This sorting substantially reduced the size of cluster detections leaving only 126 candidate groups/clusters. All of these systems were visually inspected which showed that several of these candidates were still the same real cluster but had been found at different m_c magnitudes. These remaining duplicate cluster candidates were removed by hand leaving the candidate with the highest percentile or the largest galaxy richness (if the duplicates had the same percentile). We were careful not to remove candidates that were close on the sky but appeared to be two separate entities *i.e.* a distant cluster behind a nearby group (see Section 6). This procedure resulted in a catalogue of 92 unique groups/clusters.

Table 3: The galaxy richness cutoffs determined in stage 1 of the construction of the MDS cluster sample and corresponding to the 99.5% probability threshold. These cutoffs are given as a function of the aperture radius and the magnitude of the ‘seed’ galaxy (or m_c) in the F814W filter.

m_c	radii (arcseconds)					
	10	15	20	25	30	35
17.00	2.37	2.63	3.27	3.40	3.66	3.86
17.25	2.56	2.63	3.27	3.40	4.00	4.24
17.50	2.55	4.41	5.45	5.94	6.38	5.86
17.75	2.55	4.41	4.65	4.85	5.19	5.59
18.00	2.35	3.38	3.71	4.27	5.09	6.12
18.25	2.55	3.43	4.08	4.55	5.54	7.01
18.50	2.99	3.55	4.08	4.99	5.99	7.16
18.75	3.09	3.59	4.99	5.38	6.39	7.47
19.00	3.99	6.00	5.99	6.99	9.05	9.25
19.25	3.74	5.99	5.99	6.99	8.99	9.44
19.50	4.99	8.99	8.99	10.99	12.99	14.17
19.75	4.99	10.99	11.99	13.13	16.99	18.08
20.00	4.99	7.19	9.17	12.99	17.26	20.03
20.25	5.99	8.54	9.73	11.46	14.79	17.39
20.50	4.99	7.99	9.99	11.99	15.01	18.02
20.75	5.99	8.65	11.99	13.99	17.99	20.72
21.00	5.99	8.65	10.99	14.02	17.00	20.54
21.25	5.99	8.99	11.99	15.37	19.13	22.93
21.50	6.43	9.93	12.70	15.75	20.38	25.73
21.75	6.78	10.01	13.99	17.99	22.94	29.33
22.00	7.04	11.11	15.20	20.40	26.46	32.10
22.25	7.99	12.07	17.41	23.86	31.47	40.79
22.50	9.13	14.00	19.99	27.37	36.28	44.46
22.75	9.85	14.99	21.11	30.30	40.32	51.54
23.00	10.19	16.95	24.81	36.13	47.06	63.29
23.25	10.41	19.40	30.14	41.99	57.08	76.90
23.50	12.99	22.99	34.07	47.11	65.29	89.33
23.75	13.22	23.80	35.29	50.18	70.64	92.83
24.00	14.73	24.95	37.95	52.06	69.20	94.42
24.25	17.00	29.15	45.23	60.53	80.87	107.01
24.50	17.55	32.45	51.03	68.28	88.01	112.04
24.75	18.13	32.26	50.19	72.22	99.81	129.19

4. Results

Table 4 contains the 92 overdensities detected above the 99.5% probability threshold discussed in Section 3.2. In this table we present a unique name (column 1) and the right ascension and declination (J2000) of the ‘seed’ galaxy for the cluster in columns 2 & 3. The galaxy richness within the detection aperture is given in column 4. This richness has been corrected for any area of the detection aperture outside the field *i.e.* it is scaled assuming a constant surface density of galaxies to give the expected galaxy richness if the aperture was fully within the MDS field. This explains the non-integer richnesses in Table 4. The galaxy richnesses are however not corrected for background or foreground galaxy contamination. There were three reasons for this decision. First, neither a global or a local contamination correction would have worked satisfactorily. This is because the field-to-field variations in the MDS are large thus negating a global approach. Meanwhile a local correction would have been hindered by the fact that in most cases, the presence of a cluster in a given field would have significantly skewed the galaxy counts in that field, thus leading to an over estimate for the correction. Second, $\sim 40\%$ of our overdensities have low measured richnesses, *i.e.* less than 10 members (because of the small apertures), which raises the issue of small number statistics. Finally, the MDS survey is unique because of the morphological information it contains and it becomes increasingly difficult to make a statistical correction for contamination as a function of galaxy morphology. As a first order correction to the richness, the reader may wish to multiply the richness by the bulge-to-total ratio of galaxies (Column 9 of Table 4, see below) thus obtaining the number of bulge dominated galaxies in each cluster/group. This may be a more physical richness estimate because of the density-morphology relationship *i.e.* elliptical galaxies populate the cores of clusters.

The MDS cluster richnesses may *appear* to be small compared with the richnesses quoted in the Abell catalogue (see Abell et al. 1989). However, Abell defined his cluster richnesses within an aperture of metric radius $1.5h^{-1}$ Mpc. If one scales the observed surface density of galaxies seen in our MDS clusters/groups to these larger apertures (using an appropriate cluster profile *e.g.* King), it is clear that some of our clusters would have satisfied Abell’s selection criteria; for example, HST 175525+18182 is equivalent to an Abell richness class 1 cluster. We do not provide an “Abell richness” estimate for our clusters in Table 4 because of the limitations of such an extrapolation. Moreover, we cannot compute the “Abell richness” directly as the MDS fields are too small.

In column 5, we present the detection probability for each cluster, while column 6 contains the galaxy richness that corresponds to the 99.5% cut for that particular aperture ($N_{gal\%}$ in Table 4). Column 7 is the aperture radius (in arcseconds), while column 8 is the central magnitude, m_c , of the aperture in which the cluster was detected. This magnitude, like others used elsewhere in this paper, is based on the ST system and is an analytical total magnitude derived from integrating the best fit galaxy model out to 19 half-light radii (see Ratnatunga et al. 1998). Column 9 (marked B/T) is the average for that cluster of the bulge dominated galaxies to the total number of galaxies within the detection aperture. This average has not been corrected for contamination by background, or foreground, galaxies and therefore, must be used care.

Column 10 is the WFPC2 filter used and column 11 (marked *clim*) is the magnitude completeness limit of the field as defined in Section 2 (Ratnatunga et al. 1998). Column 12 is a grade between 1 and 4 based on the visual assessment of the cluster and column 13 is the original HST target name. In total, we find 14 clusters classified with grade 1 (“excellent”), 32 as grade 2 (“good”), 29 as grade 3 (“fair”) and 17 as grade 4 (“poor”). These subjective assessments are provided to aid readers in search of a few exceptional clusters for optical follow-up. In Fig. 2, we show 9 clusters selected from Table 4 to highlight the diversity of the catalogue. In this figure, we show examples of potentially high redshift systems we have found, as well as

Table 4: The 92 MDS clusters detected above a 99.5% probability threshold as discussed in Section 3.2.

Name	RA	Dec	N_{gal}	%	$N_{\text{gal}}\%$	rad	mag	B/T	F	clim	G	Primary Target
HST 001548-16200	3.95021	-16.33396	23.00	99.53	22.94	30	21.75	0.29	i	23.92	3	L722-22-0002
HST 001557-16184	3.98791	-16.30701	10.52	99.93	7.09	10	22.75	0.33	v	24.23	1	L722-22-0014
HST 001831+16207	4.62980	16.34527	10.00	99.93	7.99	10	22.25	0.57	i	24.03	2	QSO0015+162
HST 002013+28368	5.05543	28.61357	10.00	99.99	6.79	10	21.75	0.38	i	24.59	1	QSO0020+287
HST 002458-27167	6.24412	-27.27936	9.00	99.99	7.05	10	22.00	0.20	i	24.75	2	LHS1070-B
HST 004838+85109	12.16184	85.18242	9.45	99.50	9.45	35	19.25	0.35	i	22.67	4	NGC188-AA
HST 004933-52046	12.38972	-52.07701	10.56	99.55	10.19	10	23.00	0.25	i	24.45	3	BPM16274
HST 005017-52122	12.57334	-52.20405	18.20	99.61	17.99	25	21.75	0.15	i	23.84	4	BPM16274
HST 005020-52113	12.58685	-52.18839	5.02	99.99	3.97	10	20.75	0.50	v	24.28	2	BPM16274
HST 005807-28106	14.53048	-28.17803	6.00	99.52	6.00	15	22.25	0.17	b	24.91	2	SGP1-10
HST 010957-02276	17.48903	-2.46027	5.34	99.99	5.25	35	21.00	0.21	b	24.98	4	Q0107-025B
HST 011704-08386	19.26687	-8.64425	7.78	99.99	7.28	30	19.75	0.44	v	24.06	2	Q0114-089
HST 012006+21273	20.02547	21.45598	14.96	99.69	14.00	15	22.50	0.12	i	24.05	4	0117+213
HST 013835+33043	24.64890	33.07246	8.25	99.65	7.99	10	23.00	0.50	v	24.50	3	0134+329INCA221
HST 020959-39354	32.49727	-39.59015	12.00	99.82	11.00	25	21.50	0.61	v	23.00	3	Q0207-398
HST 021002-39356	32.50857	-39.59459	16.65	99.76	15.00	15	23.50	0.30	v	25.05	4	Q0207-398
HST 021005-39350	32.52127	-39.58443	16.88	99.76	15.74	35	21.50	0.57	v	25.05	4	Q0207-398
HST 022548+27547	36.45216	27.91263	6.51	99.79	6.00	20	19.25	0.49	i	23.84	2	RWTRI-GSC-2
HST 035528+09435	58.86759	9.72577	13.00	99.99	7.99	10	22.25	0.21	i	23.41	1	HZ4
HST 035531+09441	58.88189	9.73624	8.26	99.93	6.43	10	21.50	0.31	i	23.90	4	HZ4
HST 035535+09433	58.89678	9.72319	6.05	99.90	5.10	15	20.75	0.42	v	25.01	1	HZ4
HST 045648+03529	74.20113	3.88260	7.15	99.56	7.05	10	22.00	0.50	i	24.39	3	PKS0454+039
HST 051909-45493	79.78752	-45.82233	6.61	99.72	6.05	15	21.00	0.50	v	25.34	4	PKS0518-45
HST 051910-45510	79.79485	-45.85162	21.20	99.70	19.29	30	22.25	0.20	v	25.34	4	PKS0518-45
HST 072049+71089	110.20662	71.14918	9.98	99.60	9.45	35	19.25	0.49	i	23.66	4	0716+714INCA221
HST 072442+60316	111.17674	60.52826	15.00	99.70	14.00	15	22.50	0.25	i	24.07	2	STAR-72553+60
HST 072455+60313	111.23310	60.52233	11.14	99.53	11.07	15	22.75	0.14	v	24.57	2	STAR-72553+60
HST 074239+49428	115.66546	49.71365	13.98	99.93	11.11	15	22.00	0.30	i	24.25	2	MRK79
HST 075047+14412	117.69848	14.68775	23.41	99.65	22.04	20	23.50	0.14	v	24.88	2	STAR-75117+14
HST 095007+39248	147.53330	39.41372	11.46	99.50	11.45	35	20.75	0.34	v	25.08	3	PG0947+396
HST 095012+39244	147.55212	39.40683	26.76	99.74	25.74	35	21.50	0.23	i	24.18	2	PG0947+396
HST 100456+05151	151.23347	5.25174	5.05	99.60	5.04	15	22.00	0.43	b	25.03	3	PG1001+054
HST 102722+03257	156.84344	3.42847	14.32	99.72	13.99	20	21.75	0.23	i	23.62	1	CH02
HST 111744+44177	169.43644	44.29603	5.52	99.99	5.52	20	21.50	0.20	b	24.98	3	PG1114+445
HST 112125-24558	170.35809	-24.93087	21.33	99.60	20.39	30	21.50	0.38	i	23.93	4	HD98800-5-REF
HST 115027+28496	177.61418	28.82765	10.89	99.77	10.00	10	23.75	0.29	v	25.15	2	RE1149545+284512
HST 121111+39273	182.79823	39.45605	29.04	99.95	26.99	20	24.00	0.26	v	25.49	3	NGC4151-PO
HST 121754+50123	184.47775	50.20501	17.06	99.64	16.96	15	23.00	0.45	i	24.64	4	HS-1216+5032B
HST 122332+15518	185.88700	15.86494	23.53	99.76	21.12	20	22.75	0.07	i	24.45	2	SN1979C
HST 122355+15495	185.98101	15.82555	8.00	99.80	7.05	10	22.00	0.30	i	24.27	2	1220+160
HST 123155+14163	187.98116	14.27305	46.65	99.55	46.30	30	23.75	0.13	v	25.24	2	AL-COM
HST 123639-00417	189.16295	-0.69544	9.78	99.91	7.99	10	22.25	0.17	i	24.17	2	QNY1-32
HST 123640+62111	189.16921	62.18616	24.95	99.67	23.86	25	22.25	0.29	i	24.08	3	HDF
HST 123649+62132	189.20545	62.22007	7.82	99.99	7.82	30	22.00	0.41	b	26.20	2	HDF
HST 125015+31254	192.56439	31.42368	34.00	99.99	32.20	30	23.75	0.16	b	25.53	1	CSO173
HST 125651+22062	194.21284	22.10452	9.13	99.50	9.13	10	23.50	0.25	v	25.32	2	GD153
HST 125655+22057	194.23291	22.09520	7.05	99.50	7.05	10	22.00	0.67	i	24.60	2	GD153
HST 133605+51494	204.02123	51.82415	29.18	99.99	25.92	30	22.75	0.32	v	25.12	3	UX-UMA
HST 133617-00526	204.07282	-0.87794	13.59	99.99	9.72	30	20.75	0.48	v	24.29	1	QSO-133647-004858
HST 140428+43196	211.11817	43.32792	5.59	99.99	5.59	35	17.75	0.37	i	24.75	1	IR1402+43
HST 141506+52015	213.77739	52.02592	7.26	99.61	7.05	10	22.00	0.33	i	24.30	3	141816+523430
HST 141610+52123	214.04513	52.20645	5.89	99.70	5.23	20	20.50	0.23	v	25.04	2	141613+521222
HST 141612+52133	214.05358	52.22236	5.22	99.83	5.07	20	20.25	0.41	v	25.05	4	141619+521332
HST 141613+11316	214.05788	11.52808	15.59	99.85	14.72	30	21.75	0.21	v	25.19	3	Q1413+117-D
HST 141618+52138	214.07730	52.23165	18.85	99.99	15.45	25	22.25	0.45	v	25.05	1	141619+521332
HST 141624+52155	214.10012	52.25913	11.00	99.80	9.86	10	22.75	0.17	i	25.06	3	141626+521442
HST 141637+52163	214.15461	52.27239	10.11	99.61	9.65	20	21.75	0.69	v	25.06	3	141632+521552
HST 141638+52165	214.16227	52.27623	18.53	99.67	17.99	25	21.75	0.10	i	24.37	3	141638+521702

Table 4: Continued

Name	RA	Dec	N_{gal}	%	$N_{\text{gal}\%}$	rad	mag	B/T	F	clim	G	Target
HST 141653+52210	214.22210	52.35111	13.50	99.83	11.99	25	20.50	0.34	i	24.37	1	141658+522032
HST 141654+52189	214.22910	52.31604	11.00	99.90	10.00	20	20.50	0.32	i	25.06	2	141651+521922
HST 141727+52267	214.36530	52.44579	6.85	99.53	6.79	10	21.75	0.24	i	24.37	2	141731+522622
HST 143518+24589	218.82745	24.98225	13.26	99.99	10.00	10	23.75	0.11	v	24.41	1	G166-37
HST 144152-17175	220.46995	-17.29237	19.09	99.81	17.41	20	22.25	0.28	i	24.52	3	NGC5728-EELR
HST 150620+01448	226.58519	1.74697	5.11	99.50	5.10	15	20.75	0.26	v	25.21	4	NGC5845-FOS
HST 150621+01431	226.59099	1.71872	7.00	99.50	7.00	25	19.25	0.77	i	24.05	3	NGC5845-FOS
HST 151940+23524	229.91835	23.87468	22.78	99.93	20.41	25	22.00	0.33	i	24.57	2	LB9605-NEW
HST 162413+48077	246.05638	48.12981	12.00	99.90	9.86	10	22.75	0.33	i	24.25	2	GL623-5-REF
HST 162413+48078	246.05653	48.13023	6.35	99.54	6.00	10	21.25	0.71	i	23.42	3	AC+48D1595-89
HST 163141+37375	247.92343	37.62648	14.26	99.70	13.99	20	21.75	0.45	i	24.20	2	PG1630+377
HST 171220+33354	258.08595	33.59067	11.00	99.80	10.41	10	23.25	0.11	i	24.66	3	V795-HER
HST 171223+33371	258.09734	33.61898	6.00	99.70	5.80	10	22.00	0.72	v	25.57	4	V795-HER
HST 173638+68251	264.16141	68.41998	13.21	99.88	11.51	25	21.75	0.19	v	24.27	1	BD+68D946
HST 175525+18182	268.85509	18.30430	21.85	99.99	17.99	25	21.75	0.25	i	24.68	1	NGC6500
HST 180746+45599	271.94548	45.99925	6.00	99.60	5.99	10	21.00	0.82	i	24.55	3	DQ-HER
HST 193810-46205	294.54349	-46.34241	10.10	99.62	9.86	10	22.75	0.29	i	24.46	3	QS-TEL
HST 193928-46139	294.86894	-46.23330	7.91	99.89	6.43	10	21.50	0.29	i	24.41	2	STAR-193835-46
HST 194752-41520	296.96836	-41.86737	7.00	99.80	6.00	10	21.25	0.31	i	23.86	2	V3885-SGR
HST 194754-41530	296.97723	-41.88478	8.00	99.60	7.99	10	22.25	0.50	i	23.86	3	V3885-SGR
HST 200803-48542	302.01325	-48.90438	6.18	99.70	5.99	10	21.00	0.20	i	23.74	3	2005-489INCA
HST 200811-48546	302.04916	-48.91062	15.73	99.65	15.20	20	22.00	0.14	i	23.74	2	2005-489INCA
HST 202946+09541	307.44171	9.90304	7.00	99.80	6.00	10	21.25	0.67	i	23.76	2	GL791-2
HST 213233+00161	323.14022	0.26938	6.00	99.50	6.00	10	21.25	0.39	i	23.85	3	LDS749B
HST 214823-34530	327.09744	-34.88481	6.24	99.99	5.99	15	19.25	0.70	i	23.79	2	IC5135
HST 215031+28488	327.63226	28.81387	5.54	99.84	5.39	25	18.75	0.40	i	24.23	3	BD+28D4211
HST 215112+29002	327.80405	29.00371	13.24	99.99	8.37	35	20.00	0.47	v	24.84	3	BD+28D4211
HST 215115+28599	327.81565	28.99922	8.37	99.87	7.05	10	22.00	0.14	i	24.17	4	BD+28D4211
HST 215118+28587	327.82690	28.97907	10.04	99.99	10.02	25	22.25	0.27	b	25.31	3	BD+28D4211
HST 215125+29001	327.85699	29.00236	29.40	99.99	25.74	35	21.50	0.43	i	24.13	3	BD+28D4211
HST 215128+28581	327.86881	28.96943	12.00	99.86	10.02	15	21.75	0.27	i	24.13	2	BD+28D4211
HST 215137+28590	327.90569	28.98339	14.35	99.57	14.00	15	22.50	0.38	i	24.41	2	BD+28D4211
HST 225657-36342	344.23860	-36.57086	15.85	99.55	15.76	25	21.50	0.15	i	24.56	1	IC1459-NUC
HST 230425+03051	346.10657	3.08629	7.33	99.60	7.09	10	22.75	0.50	v	24.59	4	PG2302+029

candidates for nearby compact groups of galaxies. We also show that clusters can be detected near the edge of the WFPC2 field-of-view (bottom right) as well as clusters spanning all 4 WFPC2 chips (bottom center).

In order to estimate photometric redshifts for the galaxy overdensities presented here, further color information is required as demonstrated by Connolly et al. (1995). Estimated redshifts are in the range from about 0.3 to 1.0, with a mean of 0.7 and a rms of about 0.25.

We have cross-correlated the clusters in Table 4 against existing distant cluster catalogues (Gunn et al. 1986, Couch et al. 1991, Postman et al. 1996) and found no overlap. This results from a combination of our decision to avoid known clusters (see Table 8), and the fact that the MDS fields are located between 4 and 14 arcmins away from the primary target (observed with FGS, FOS or FOC). We also searched the NASA/IPAC Extragalactic Database (NED) for all possible matches within the aperture radius of each cluster (given in Table 4). In total, 5 MDS clusters were coincident with NED sources and these 5 are presented in Table 5 and discussed in more detail below.

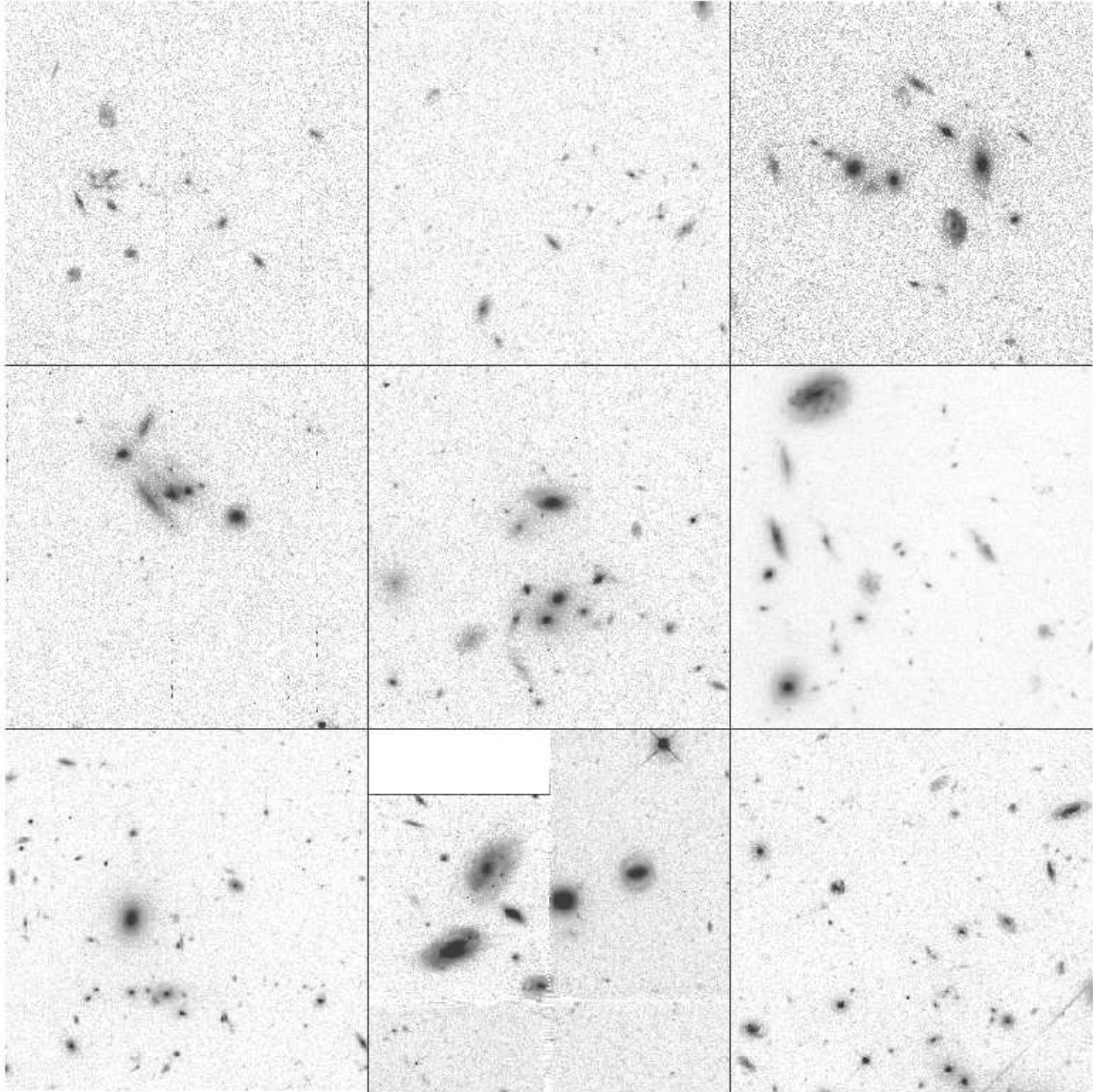


Fig. 2.— We present here nine examples of clusters and groups found as part of the HST MDS cluster sample. The boxes are 30 arcseconds square and the passbands are the same as given in Column 10 of Table 4. On the top row, from left to right, we present HST 035528+09435, HST 115027+28496 and HST 102722+03257. On the middle row, from left to right, are HST 005021-52113, HST 002013+28366 and HST 123648+62132. On the bottom, from left to right, are HST 141617+52137, HST 140428+43196 and HST 133617-00529.

Table 5: The five MDS clusters with a NED coincidence (see text)

Name	Comments
HST 001831+16208	Close to RXJ0018.3+1618, RXJ0018.8+1602 and CL0016+16 all at $z \simeq 0.55$. Symmetric double radio source MRC 0015+160, with a 30 arcsecond error circle (95% confidence), within cluster aperture (see Douglas et al. 1996). Faint X-ray emission associated with cluster and radio source (see Fig. 1 of Hughes et al. 1995).
HST 010957–02276	Two galaxies within aperture with redshifts $z = 0.205$ & $z = 0.298$.
HST 123640+62111	Flanking the Hubble Deep Field.
HST 123649+62132	Hubble Deep Field. Six redshifts in aperture, three at $z = 0.475$. (see text and Fig. 2)
HST 141727+52267	Coincident with galaxy CFRS 14.1496 $z = 0.899$ (see Lilly et al. 1995). Galaxy CFRS 14.1501 also within aperture radius and is a radio source (Hammer et al. 1995)

HST 010957-02276 has a galaxy richness of 5.34 over a 35 arcsecond radius aperture and is described as “poor”. It has two measured redshifts which are significantly different.

HST 123649+62132 is shown in Fig. 2 and is at the center of the HDF. There are now 6 measured galaxy redshifts within the aperture radius (from the HDF spectroscopic follow-up, see Cohen et al. 1996) of which 3 are in agreement; $z = 0.475, 0.475$ & 0.478 with all three being ellipticals. The remaining 3 redshift measurements are $z = 0.199, 0.958$ & 0.749 with all three galaxies being spirals or irregulars. The finding of this overdensity is thus essentially vindicated, but also illustrates the contaminating effect of galaxies along the line of sight.

HST 123640+62111 was detected in the HST fields that flank the Hubble Deep Field (see Fig. 3).

The central galaxy of HST 141727+52267 is coincident with CFRS 14.1496 at $z = 0.899$ from the Canada–France Redshift Survey (CFRS; see Lilly et al. 1995) and this group is shown in Fig. 4. Also within the aperture is CFRS 14.1501 which is identified as a radio source by Hammer et al. (1995).

HST 001831+16208 is approximately 2 arcmins from RXJ0018.3+1618. This group, discovered by Hughes, Birkenshaw & Huchra (1995), is companion to the famous CL0016+16 cluster at $z = 0.546$ (Koo 1981). In addition to RXJ0018.3+1618, yet another group of galaxies was recently found close-by, RXJ0018.8+1602 (Connolly et al. 1996), at the same redshift (Connolly et al. 1997; Hughes & Birkenshaw 1997) thus raising the possibility that these clusters/groups are part of a supercluster at $z = 0.55$. This new MDS cluster potentially adds a further cluster/group to this high-redshift supercluster.

HST 001831+16208 is a compact group with $N_{\text{gal}} = 10.00$ within a radius of 10 arcseconds ($\sim 75h^{-1}$ kpc diameter at $z = 0.6$) and appears to be coincident with a faint X-ray source as seen in Figure 1 of Hughes et al. (1995). HST 001831+16208 is very close to the large cross – south of the main CL0016+16 cluster – which marks the position of a known radio source (MRC 0015+160; see Douglas et al. 1996). Figure 5

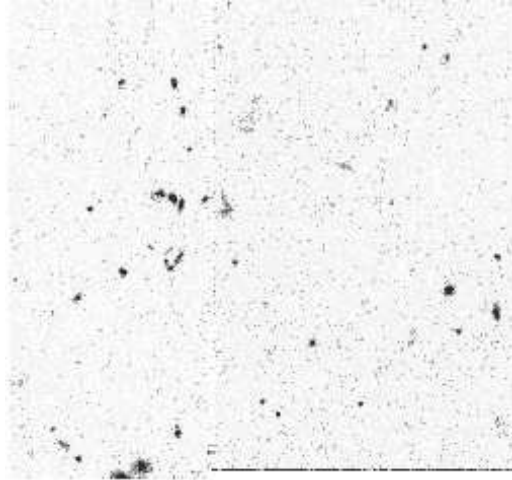


Fig. 3.— This is a greyscale picture of cluster HST 123640+62111 which is located in the flanking fields of the Hubble Deep Field. The box is 30 arcseconds square and is in the F814W passband.

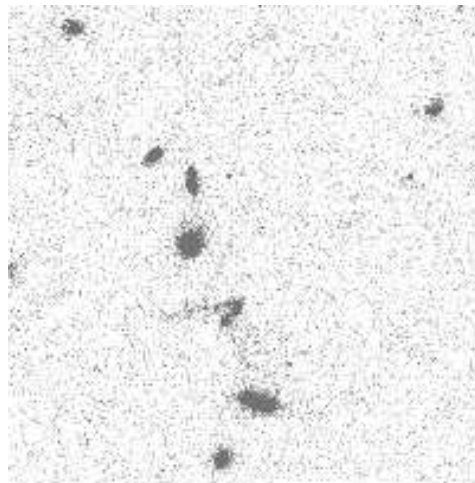


Fig. 4.— This is a greyscale picture of cluster HST 141727+52267 which has one measured redshift (0.899) within it's detection aperture (see text). The box is 30 arcseconds square and is in the F814W passband.

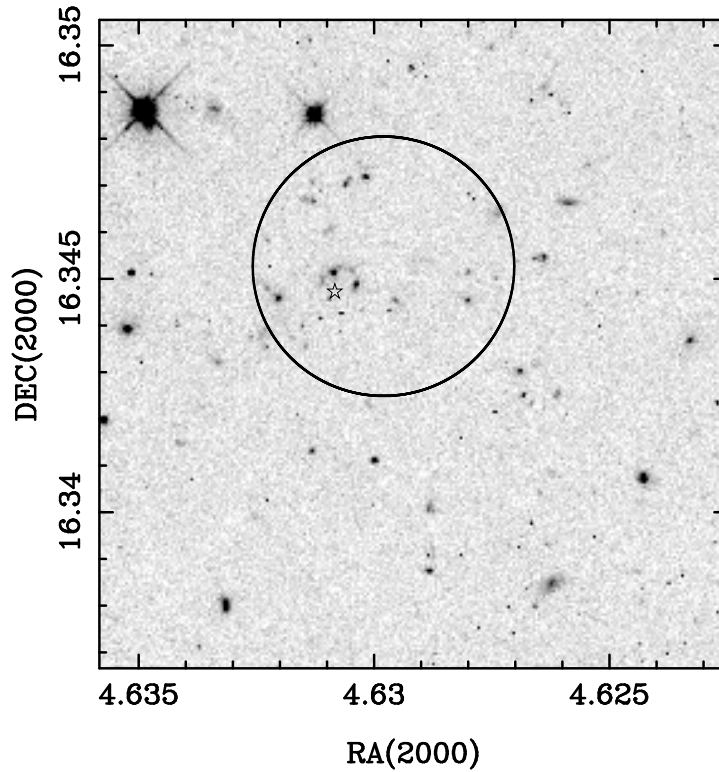


Fig. 5.— This is a greyscale picture of HST 001831+16208 in the F814W filter. The quality of the optical data is poor since this MDS field received less than 1 hour of exposure time. The aperture this cluster was detected in is shown (Table 4) and the position of the known radio source, MRC 0015+160, is marked with a star. The image is slightly rotated.

shows this new cluster and the position of the aforementioned radio source.

It is worth noting that in addition to the ROSAT PSPC data used by Hughes et al. (1995), a deep ROSAT HRI pointing towards CL0016+16 also overlaps HST 001831+16208. Even though the exposure time is longer, the X-ray source seen in the PSPC data, which is coincident with both HST 001831+16208 and MRC 0015+160, does not appear to be detected in the HRI data. Such a non-detection may indicate that the observed PSPC X-ray emission is slightly extended thus lowering the X-ray surface brightness of the source below the higher background level in the HRI data. Follow-up observations are needed to conclusively determine if this group has associated extended X-ray emission.

5. Simulations

We discuss here the simulations we have performed to assess the likely contamination of the MDS cluster sample by projection effects *i.e.* how many of the 92 clusters in Table 4 are real and how many are superpositions of galaxies along the line of sight. In a future paper, we will examine the completeness of the survey – the percentage of true clusters in the universe detected as a function of richness, redshift and the selection parameters – and define the volume sampled by the MDS cluster sample.

Table 6: The number of real cluster detections, as a function of m_c and aperture radius, versus the average number of detections in the simulated MDS cluster catalogs. [Note: we have used all 126 detections in this table (Section 3.2) as the multiple detections cannot be removed by hand, unlike the real MDS catalog which resulted from the reduction of the 126 detections to 92 in Table 4]. The first number within parentheses is the average number of detections for the shuffled magnitude simulations discussed in the text. The second number within parentheses is the average number of detections for the randomized coordinate simulations. 3000 trials were run for both sets of simulations.

m_c	radius arcseconds					
	10	15	20	25	30	35
17.5	0 (0.000:0.000)	0 (0.000:0.001)	0 (0.002:0.004)	1 (1.970:1.098)	0 (0.264:0.256)	1 (0.373:0.229)
18.5	0 (0.000:0.000)	0 (0.018:0.028)	1 (0.072:0.231)	1 (0.196:0.798)	1 (0.272:0.946)	2 (0.367:1.166)
19.5	2 (0.108:0.132)	1 (0.000:0.023)	3 (0.108:0.278)	1 (0.216:0.425)	0 (0.023:0.080)	4 (0.431:0.869)
20.5	2 (0.795:1.371)	0 (0.132:0.183)	1 (0.139:0.178)	2 (0.264:0.289)	1 (0.134:0.138)	1 (0.375:0.315)
21.5	9 (2.154:2.630)	1 (0.894:1.136)	4 (1.013:1.234)	9 (1.881:2.063)	5 (1.956:1.918)	7 (2.356:2.489)
22.5	16 (5.814:4.443)	15 (3.195:2.279)	5 (3.885:3.591)	4 (3.090:2.693)	0 (2.313:2.186)	15 (7.311:7.333)
23.5	3 (3.469:1.749)	2 (1.327:0.706)	0 (1.283:0.738)	1 (0.542:0.268)	1 (0.349:0.363)	0 (1.291:0.318)
24.5	1 (0.121:0.514)	0 (0.162:0.406)	2 (0.215:0.630)	0 (0.000:0.000)	0 (0.000:0.000)	0 (0.000:0.000)

To determine the contamination level, we performed two sets of simulations. The first of these involved taking the MDS galaxy data and “shuffling”, at random, the magnitudes of the galaxies. This produced fake MDS catalogues with the exact same angular correlations as the real data, and the same magnitude distributions, but with very different magnitude correlations. These simulations help to test the strength of the magnitude correlations for the real clusters/groups.

The second set of simulations involved making fake MDS galaxy catalogues by randomizing the coordinates of the galaxies within each field. This ensures that we have the same number and type of galaxies (bulge and disk dominated) per field and tests the strength of the observed angular correlations. We note that these latter simulations are somewhat naive since they do not fully account for the known angular galaxy correlations (Collins, Nichol & Lumsden 1992). However, with these simulations we are only testing the significance of galaxy angular correlations within a limited magnitude range (each aperture is only 2 magnitudes wide).

These fake, or simulated, MDS catalogues were searched for clusters using the same methodology as detailed in the previous section. The main difference was that the richness cutoffs, like those given in Table 3, were not re-computed but the same cutoffs as determined for the real data were used.

In Table 6, we present the results of these simulations based on searching the fake MDS catalogues (3000 for both sets of simulations). This table shows the real number of cluster detections, as a function of their detection aperture radius and m_c , together with the average number of detected clusters in the fake catalogues (we have coarsely re-binned the values of m_c into bins of width 1 magnitude). This helps to demonstrate the expected rate of contamination as a function of these two detection parameters and will help the reader to determine the significance of any particular cluster detection compared to others. For example, in Table 6 the two clusters detected at $19 < m_c < 20$ and radius = $10''$ (0.108:0.132) are much more likely clusters than the two detected at $23 < m_c < 24$ and radius = $15''$ (1.327:0.706) because of the

Table 7: A summary of all simulations carried out to understand our cluster-finding algorithm. The left-hand column presents the type of simulation carried out – magnitude-shuffling or the randomizing of the coordinates – as well as the HST passband used.

Type of simulation	Morphology		
	All Galaxies	Bulge	Disk
F450W & magnitudes	54%	34%	60%
F450W & coordinates	71%	31%	83%
F606W & magnitudes	51%	44%	50%
F606W & coordinates	48%	40%	48%
F814W & magnitudes	53%	40%	55%
F814W & coordinates	45%	38%	46%

relative increase in the average number of false detections in both sets of simulations (given in brackets).

A close examination of Table 6 shows that the number of fake clusters detected as a function of m_c and aperture radius is correlated with the actual number of detections in that bin. At bright magnitudes this is due to the fact that a real cluster in the data can add a significant number of galaxies to that magnitude bin and therefore, it will be detected again and again in the fake datasets. In such a case, the average number of fake detections in these bright magnitude bins is overestimated compared with a truly random process. At fainter magnitudes, the volume of the survey is increasing along with the number of galaxies in the MDS. Therefore, one would expect to find more clusters in both the real dataset and in the fake catalogues.

In addition to simulating our false detection rate, we also carried out simulations to test our cluster finding algorithm and our original hypothesis that centering on bulge dominated galaxies increases our success rate in detecting real clusters/groups. For these extra simulations, we again computed the ratio of real galaxy overdensities detected in the MDS data versus the average number of fake clusters detected in the simulated catalogues (both shuffled magnitudes and randomized coordinates). The crucial difference for these extra simulations was that we centered on disk dominated galaxies, as opposed to bulge dominated galaxies above, and then repeated the exercise by centering on all galaxies regardless of their morphological classification.

In Table 7, we present a summary of all these simulations. The table shows the type of simulation carried out, magnitude shuffling or coordinate randomization, along with the bandpass used and the morphology of the centered galaxy *i.e.* bulge dominated, disk dominated or all galaxies regardless of the morphological classification. The percentages given in this table are the ratios of the average number of detections in these simulations compared to the number of detections in the real overdensity database. Table 7 demonstrates that by centering on bulge dominated galaxies, the overall expected false-detection rate should be between 30% to 40%; in other words, *at least* 60% of the MDS clusters are likely real overdensities. This is smaller than the false-detection rates estimated by van Haarlem et al. (1997) for the Abell catalogue, but comparable to the estimate of Lucey (1983).

Table 7 also shows that the false detection rate increases substantially for the other methodologies *i.e.* centering on all galaxies as opposed to just bulge dominated galaxies. The worst case is centering on disk dominated galaxies where the percentage of false detections, compared to real detections, is $> 50\%$. It is not surprising that the numbers given in Table 7 for all galaxies closely follows those given for disk

dominated galaxies as 80% of all MDS galaxy morphologies are disk dominated.

6. Selection Function

The methodology outlined in this paper allows us to determine the selection function of the MDS cluster sample. This is an important quantity as it will enable us to estimate the sampled volume. We present here an empirical discussion of the selection function.

One of the main caveats of the MDS cluster sample, as presented in Table 4, is that it has been selected using morphological criteria. This may be unsuitable at high redshift if the morphologies of cluster galaxies are shown to evolve. Moreover, our algorithm implicitly assumes that the angular galaxy correlation functions for bulge dominated and disk dominated galaxies are the same, which may not be true. Our simulations have shown that our morphology-based methodology has helped to increase the ratio of real clusters detected compared with spurious systems (see Table 7). However, to alleviate some of these concerns, we have made available via the MDS World-Wide-Web homepage (<http://astro.phys.cmu.edu/mds/>), a complete list of detected overdensities regardless of the morphology of the central galaxy. The reader is warned that there is a higher level of contamination in this catalogue (see Table 7). The original galaxy catalogues used in the search (in all three passbands) are made available, together with all 126 clusters detected after the first pass through the candidates following removal of duplicates (see Section 3.2) *i.e.* we provide the 34 clusters (126 – 92) that were altered by hand as we believed they were also duplicates. Also presented are the galaxy richness cutoffs for the F450W and F606W passbands (like those given in Table 3), a copy of the computer software (fortran) used and a list of the MDS fields searched. These data are provided to facilitate checks of our clusters and methodology.

Another potential bias with the HST MDS cluster survey is the small field-of-view of the WFPC2 instrument. Clusters of galaxies are large objects on the sky and typically the core radius of clusters is larger than the WFPC2 field size; for example, at $z = 1.25$, near the minimum in the angular diameter-redshift relation for currently popular cosmological models, a typical cluster core radius ($250h^{-1}$ kpc) subtends ~ 1 arcmin on the sky which is larger than any aperture we use in our analysis. Therefore, the reader is warned that the HST MDS cluster survey is certainly biased towards compact systems.

To investigate this potential bias, we processed HST WFPC2 archival data on known distant clusters using the same algorithm as described above. We did not redetermine the thresholds, but used the same ones as discussed above and presented in Table 3. We also sorted the clusters and removed overlapping systems as discussed in Section 3.2. The cluster fields used in this analysis are shown in Table 8 where we present the MDS field identifier, the name of the target cluster, the name of the Principal Investigator and the redshift of the cluster (taken from the NED database). We also include the number of cluster detections in each of these fields using our MDS cluster-finding algorithm. We note that this number of cluster detections still includes some multiple detections because we have not merged the cluster lists from different passbands. Therefore, it is an upper limit and should be used for illustrative purposes only.

The fields in Table 8 were excluded from the main MDS cluster survey analysis because they would have biased the serendipitous nature of our survey as well as dominating our statistical distributions because of the sheer number of cluster detections; these cluster fields are significantly overdense compared to the normal MDS fields and as a result, we find hundreds of candidate clusters in these fields. In Table 9, we give the average number of clusters/groups detected, as a function of passband, in both the targetted cluster fields (Table 8) and the main MDS fields. On average, we detect ~ 25 times more clusters/groups

Table 8: WFPC2 archival data towards known clusters of galaxies. We present the (internal) MDS field identifier, the primary target name, the name of the Principal Investigator, the number of HST pointings towards the cluster, a redshift (if known) from the NED database, any alternative name for the cluster, and the number of detections for this cluster using the HST MDS cluster survey algorithm.

MDS Field Identifier	Cluster Name (in HST Arcive)	No. of Pointings	Name of PI	Redshift (if known)	Comments (alt. names)	No. Detections
u2841–u2842	GAL-CLUS1322+3027	2	Westphal	0.751	GHO 1322+3027	15
u2845	GAL-CLUS1603+4313	1	Westphal	0.895	GHO 1602+4312	1
u29g1–u29g2	GAL-CLUS-002635+170944	2	Turner	0.390	ZwCl 0024.0+1652	40
u2c41	GAL-CLUS-001558+1609	1	Dressler	0.541	Cl0016+16	25
u2c42	GAL-CLUS-005431–2756	1	Dressler	0.56	J1888.16CL	13
u2c44	GAL-CLUS-041234–6558	1	Dressler	0.51	F1557.19TC	25
u2c47	GAL-CLUS-093942+47	1	Dressler	0.402	A851	16
u2c48	A370	1	Dressler	0.373		14
u2fq1	A2390	1	Fort	0.231	RX J21535+1741	31
u2fq2	CL2244-02	1	Fort	0.330	EXSS 2244.6–0220	16
u2gk1–u2gk2	A665	2	Franx	0.181		43
u2uj1–u2ujb	GAL-CLUS-135951+623105	10	Franx	0.328	MS 1358.4+6245	84
u2ul1	GAL-CLUS-030533+171005	1	Illingworth	0.424	MS 0302.7+1658	5
u2ul2	GAL-CLUS-030518+172838	1	Illingworth	0.425	MS 0302.5+1717	9
u2ul4	GAL-CLUS-214012–233927	1	Illingworth	0.313	MS 2137.3–2353	13
u2um1	GAL-CLUS-073924+702311	1	Fevre			2
u2vk2	GAL-CLUS-023143+004844	1	Postman			2
u2w91–u2w98	A1689	4	Kaiser	0.181		43
u3062	MS1054–03	1	Donahue	0.823		26
u3063	MS1137+66	1	Donahue	0.782		34
u30h1	3C215	1	Ellingson	0.411	QSO field	6
u30h2	5C2.10	1	Ellingson	0.478	QSO field	14
u30h3	3C281	1	Ellingson		QSO field	5
u34e1	GAL-CLUS1322+3115	1	Westphal	0.755	GHO 1322+3114	13
u34m2	FIELD-0336–3645	1	Grillmair		Fornax $z = 0.0046$	1
u34m3	FIELD-0338–3523	1	Grillmair		Fornax $z = 0.0046$	4

Table 9: The number of clusters detected in WFPC2 fields towards known clusters of galaxies (Table 8). We give the passband used in the analysis, the number of cluster fields exposed to that passband, the total number of clusters detected in those fields and the average number of clusters detected per field (labelled Av. detection rate 1). For comparison, we present the average number of clusters detected per field in the main MDS cluster survey (labelled Av. detection rate 2).

Filter	No. Cluster Fields	No. Clusters Detected	Av. Detection Rate 1	Av. Detection Rate 2
F450W (b)	4	26	6.5	0.4
F606W (v)	36	280	7.8	0.3
F814W (i)	43	388	9.0	0.4

in known cluster fields than in general MDS fields; this is the result of the fact that every elliptical in these known clusters produces a candidate MDS cluster. This exercise demonstrates that our algorithm is very sensitive to a wide range of clusters, both in redshift, $\sim 0.2 < z \lesssim 0.9$, and richness *i.e.* from A665, which is one of the richest clusters in the Abell catalog, to the proposed group around 3C215 (Ellingson & Yee 1994). Therefore, we may not be severely biased against clusters which are much larger than the WFPC2 instrument *i.e.* low redshift systems. If one of the MDS fields had accidentally fallen upon such a low-redshift cluster, Tables 8 & 9 demonstrate that we would have detected it.

We note here that the data presented in Tables 8 & 9 is scientifically interesting beyond simple tests of our algorithm. This work allows us to put known, well studied clusters into the same statistical framework as the rest of the MDC Cluster Survey. For example, it allows us to assess the statistical significance of any clusters found in these fields compared to the cluster population as a whole.

Finally, in Figure 6 we show the distribution of cluster detections plotted as a function of their WFPC2 instrumental coordinates. This exercise demonstrates that our algorithm detects cluster candidates evenly throughout the WFPC2 field; it is not biased towards preferentially finding clusters near the field center. The algorithm finds clusters in the corners of the field as well as across CCD boundaries. This exercise also allowed us to determine the effective area of the WFPC2 instrument to our cluster search. Accounting for the decrease in sensitivity towards the edges of the field while including the Planetary Camera, the effective search area was computed to be 4.27 arcmins².

7. Discussion and Conclusions

In this paper, we present the results of a search for galaxy overdensities within the HST Medium Deep Survey. This search was fully automated and has an objective selection function. The 92 clusters found are presented in Table 4 and are the richest, most significant overdensities within the MDS survey.

A close examination of Table 4 demonstrates that we have potentially found some very high redshift clusters/groups, with about 25% of the sample having estimated redshifts $z \gtrsim 0.9$. If we restrict ourselves to considering only candidates rated as “excellent” or “good”, then we still have about 10% of our systems above this redshift. This significantly increases the number of potential cluster candidates above this particular redshift, since the PDCS has only 9 cluster candidates at $z_{est} > 0.9$. These combined optical

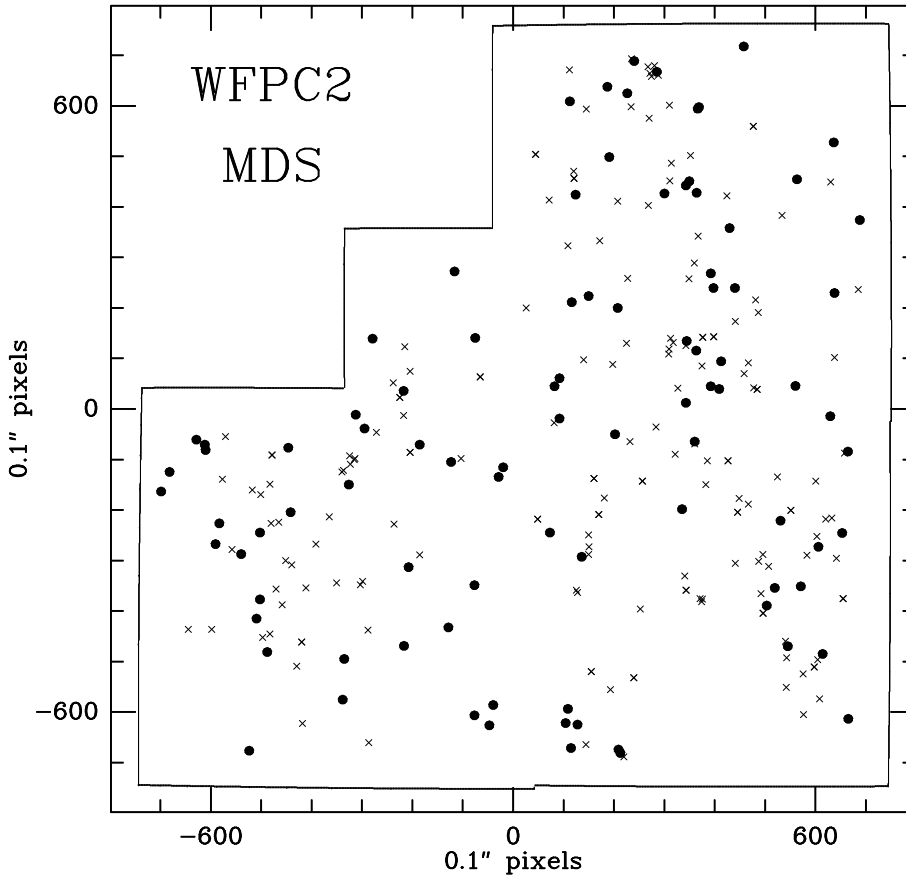


Fig. 6.— The pixel coordinate of cluster detections within the WFPC2 field-of-view. Shown are the 3 main CCD chips as well as the Planetary Camera in the top-left quadrant. The \bullet symbols are all sorted cluster detections in the F814W data, *i.e.* removal of overlapping systems, while the \times symbols are the unsorted F814W detections. The thin solid line outlines the nominal boundary of the WFPC2 instrument (a total area of 4.75arcmins^2). As expected, we are insensitive to cluster detections close to the edges of the field-of-view (we demand that 75% of the detection aperture is within the MDS field). We have computed the effective cluster search area of a WFPC2 field using this figure and it is 4.27arcmins^2 .

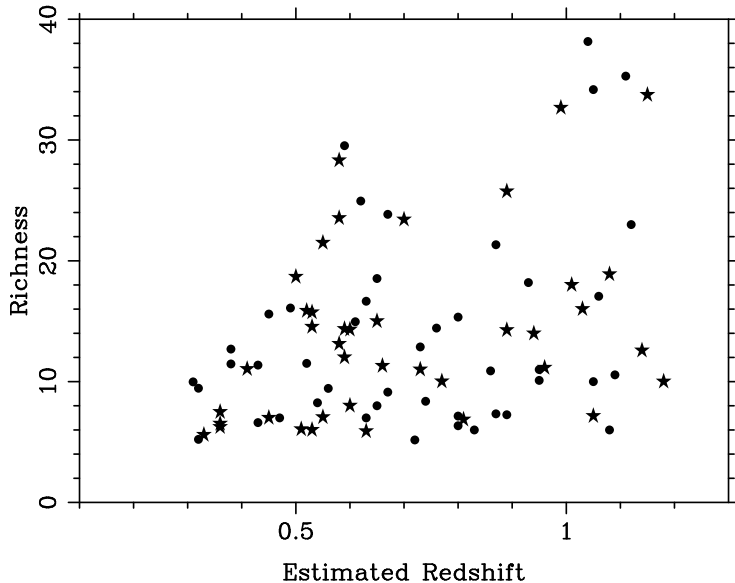


Fig. 7.— The richness of the MDS clusters versus their estimated redshifts. The \star symbols are clusters classified as “excellent” or “good” (see Table 4), while the \bullet symbols are the remaining clusters.

catalogues may provide excellent targets for studies of cluster and galaxy evolution.

We note here that the PDCS covers an area of 5deg^2 , a factor of 10 greater than the MDS HST cluster sample, yet we find a comparable number of $z > 0.9$ clusters. This apparent discrepancy in the surface density of such systems should not be over interpreted, as it is simply a reflection of the different photometric limits of the two surveys (PDCS is complete to only $I_4 = 22$). Also, it is a reflection of the different cluster-finding algorithms: Postman et al. did not attempt to search for clusters below an Abell richness class 1 at such high redshift, so the PDCS is only complete in the redshift range $0.2 < z < 0.6$.

In Figure 7, we show the richness of our systems versus redshifts roughly estimated using $(V - I)$ color, following the prescription of Im (95). This figure indicates that at lower redshifts, we are only detecting poor systems *i.e.* groups. This is to be expected since the volume sampled at these lower redshifts is small and therefore, we are insensitive to rich clusters which have a low space density. At higher redshift, however, we do appear to be detecting richer systems as our volume increases. One caveat to this statement is that at higher redshift the amount of line-of-sight contamination increases as well.

We have performed extensive Monte Carlo simulations to help understand our cluster-finding algorithm and estimate our false-detection rate. These simulation have shown that $> 60\%$ of the MDS cluster sample are real spatial overdensities and not due to chance projections on the sky. This percentage is in good agreement with our visual impression of these systems where we have classified 50% of the MDS clusters as either “excellent” or “good” (see Table 4). Our simulations also show that this percentage decreases if one widens the search for clusters to disk dominated galaxies or all galaxies. This demonstrates that our methodology does help to minimize the rate of false detections and increases our sensitivity to real groups/clusters.

We cross-correlated the MDS cluster sample against known catalogues of extragalactic objects including previous catalogues of distant clusters (Gunn et al. 1986; Couch et al. 1991; Postman et al. 1996). Only five MDS clusters had a coincidence with a known source, none of which were known clusters. This demonstrates that most of our MDS clusters are new, previously unknown systems. Both HST 010957-02276 and HST 123648+62132 have multiple galaxy redshift measurements which indicate that the former is probably spurious while the latter cluster is a bound group (in the HDF field). HST 141727+52267 has one galaxy redshift measurement of $z = 0.899$, while HST 001830+16208 is close on the sky to the massive cluster CL0016+16 thus supporting the hypothesis that these clusters and groups are part of a supercluster at $z = 0.55$ (Connolly et al. 1996).

The MDS cluster sample will be useful to address key issues in cluster research. First, in Table 4, we present the ratio of the bulge dominated galaxies in our systems compared to the total number of galaxies. This ratio indicates the overall morphological constitution of these overdensities and, in future, can be used to probe the evolution of clusters/groups as a function of epoch *i.e.* to help address the Butcher & Oemler (1984) effect and the density–morphology relation (Dressler 1980). However, such analyses will require redshift measurements before they can be conclusive.

Finally, the volume of the MDS cluster sample can be estimated via extensive Monte Carlo simulations, thus allowing the number density of our systems to be calculated. This may possibly provide a constraint on structure formation models and on the value of Ω (see Blanchard & Bartlett 1997, Reichart et al. 1998).

8. Acknowledgements

The data presented here are from the HST Medium Deep Survey project, and we acknowledge the other members of the MDS team (see author list in Griffiths et al. 1994). This work is based on observations taken with the NASA/ESA *Hubble Space Telescope* obtained at the Space Telescope Science Institute, which is operated by the Association of Universities for Research in Astronomy, Inc. The HST Medium Deep Survey has been funded by STScI Grants GO 2684.0X.87A and GO 3917.0X.91A, and we also acknowledge support from STScI Grant GO 7536 for archival analysis of clusters. We thank Kathy Romer, Jeff Peterson and Andy Connolly for helpful discussions about this work and for constructive comments on earlier drafts of this paper. We are grateful to Jack Hughes for discussions concerning the ROSAT HRI data towards HST 001831+16208. We thank the referee, Francisco Castander, for his constructive comments which resulted in many improvements to the paper. EJO and KUR were partially supported by JPL contract 959501 for WFPC2 GTO team science and RCN was partially supported on NASA grant NAG5-6548. This research has made use of the NASA/IPAC Extragalactic Database (NED) which is operated by the Jet Propulsion Laboratory, California Institute of Technology, under contract with the National Aeronautics and Space Administration.

REFERENCES

- Abell, G. O., 1958, ApJS, 3, 211.
Abell, G. O., Corwin, H. G. & Olowin, R. P., ApJS, 70, 1.
Blanchard, A., & Bartlett, J. G., 1997, A&A, 332L, 49.
Butcher, H. R., & Oemler, A., 1978, ApJ, 219, 18.

- Cohen, J. G., Cowie, L. Hogg, D. W., Songaila, A., Blanford, R., Hu, E. M., & Shopbell, P., 1996, *ApJ*, 471, L5.
- Collins, C. A., Nichol, R.C, & Lumsden, S. L., 1992, *MNRAS*, 254, 295.
- Connolly, A. J., Csabai, I., Szalay, A. S., Koo, D. C., Kron, R. G. & Munn, J. A., 1995, *AJ*, 110, 2655
- Connolly, A. J., Szalay, A. S., Koo, D. C., Romer, A. K., Holden, B. P., Nichol, R. C., & Miyaji, T., 1996, *ApJ*, 473, L69
- Connolly, A. J., Szalay, A. S., Romer, A. K., Nichol, R. C., Holden, B. P., Koo, D. C., & Miyaji, T., 1997, in *Proceedings of the 18th Texas Symposium in Relativistic Astrophysics*, in press. astro-ph/9702025.
- Couch, W. J., Ellis, R. E., Sharples, R. M., & MacLaren, I., 1991, *MNRAS*, 249, 606.
- Dickinson, M., 1997, *Proceedings of ESO/VLT meeting “Galaxy Scaling Relations: Origin, Evolution and Applications”*. ed. L. da Costa. astro-ph/9703035
- Douglas, J. N., Bash, F. N., Bozayan, A. F., Torrence, G. W., & Wolfe C., 1996, *AJ*, 111, 1945.
- Dressler, A., 1980, *ApJ*, 236, 351.
- Ellingson, E. & Yee, H. K. C. 1994, *ApJS*, 92, 33.
- Frenk, C. S., White, S. D. M., Efstathiou, G., & Davis, M., 1990, *ApJ*, 351, 10.
- Griffiths, R. E., Ratnatunga, K. U., Neuschaefer, L. W., Casertano, S., Im, M., Wyckoff, E. W., Ellis, R. E., Gilmore, G. F., Elson, R. A. W., Glazebrook, K., Schade, D. J., Windhorst, R. A., Schmidtke, P. C., Gordon, J. M., Pascarelle, S. M., Illingworth, G. D., Koo, D. C., Bershadsky, M. A., Forbes, D. A., Phillips, A. C., Green, R. F., Sarajedini, V., Huchra, J. P. & Tyson, A. J., 1994, *ApJ*, 437, 67.
- Gunn, J. E., Hoessel, J. G., & Oke, J. B., 1986, *ApJ*, 306, 30.
- Hammer, F., Crampton, D., Lilly, S. J., Le Fevre, O., & Kenet, T., 1995, *MNRAS*, 276, 1085.
- Hickson, P., 1997, *ARA&A*, 35, 357.
- Huchra, J. P., Henry, J. P., Postman, M., & Geller, M. J., 1990, *ApJ*, 365, 66.
- Hughes, J. P., Birkenshaw, M., & Huchra, J. P. 1995, *ApJ*, 448, L93
- Hughes, J. P., & Birkenshaw, M., 1997, *ApJ*, 497, 645.
- Im, M., 1995, Ph.D thesis, Johns Hopkins University
- Im, M., Griffiths, R. E., Ratnatunga, K. U., & Sarajedini, V., 1996, *ApJ*, 461, L79
- Kawasaki, M., Shimasaki, K., Doi, M., & Okamura, S., 1997, *A&AS*, 130, 567.
- Kepner, J., Fan, X., Bahcall, N., Gunn, J. E. & Lupton, R., 1998, *ApJ*, astro-ph/9803125
- Kodama, T., Bell, E. F. & Bower, R. G., 1998, *MNRAS*, astro-ph/9806120
- Koo, D. C., 1981, *ApJ*, 251, L75
- Lidman, C. E., & Peterson, B. A., 1996, *AJ*, 112, 2454

- Lilly, S. J., Hammer, F., Le Fevre, O., & Crampton, D., 1995, *AJ*, 455, 75.
- Lucey, J. R., 1983, *MNRAS*, 204, 33.
- Lumsden, S. L., Nichol, R.C, Collins, C. A., & Guzzo, L. 1992, *MNRAS*, 258, 1.
- Postman, M., Huchra, J. P. & Geller, M. J., 1992, *ApJ*, 384, 404.
- Postman, M., Lubin, L. M., Gunn, J. E., Oke, J. B., Hoessel, J. M., Schneider, D. P., & Christensen, J. A., 1996, *AJ*, 111, 615.
- Press, W. H, & Schechter, P., 1974, *ApJ*, 187, 425.
- Ratnatunga, K. U., Griffiths, R. E., Casertano, S., Neuschaefer L. W. & Wyckoff, E. W., 1994, *AJ*, 108, 2362.
- Ratnatunga, K. U., Griffiths, R. E., Ostrander, E. J., 1998, in preparation (see <http://astro.phys.cmu.edu/mds/mle/>)
- D. E. Reichart, D.E., Nichol, R.C., Castander, F.C., Burke, D., Romer, A.K., Holden, B.P., Collins, C.A. & Ulmer, M.P., *ApJ*, astro-ph/9802153
- Richstone, D., Loeb, A. & Turner, E. L., 1992, *ApJ*, 393, 477.
- Roche, N., Ratnatunga, K. U., Griffiths, R. E. & Im, M., 1998, *MNRAS*, 288, 200
- Slezak, E., Bijaoui, A & Mars, G., *A&A*, 227, 301
- Williams, R. E. et al. 1996, *AJ*, 112, 1335
- van Haarlem, M. P., Frenk, C. S., & White, S. D. M., 1997, *MNRAS*, 287, 817.
- Zwicky, F., Herzog, E., Wild, P., Karpowicz, M. & Kowal, C. T. 1968, *Catalogue of Galaxies and Clusters of Galaxies* (California Institute of Technology, Pasadena)